Cell Reports, Volume *43*

Supplemental information

Hippocampal astrocytes induce sex-dimorphic effects on memory

Samantha M. Meadows, Fernando Palaguachi, Minwoo Wendy Jang, Avital Licht-Murava, Daniel Barnett, Till S. Zimmer, Constance Zhou, Samantha R. McDonough, Adam L. Orr, and Anna G. Orr

Supplemental Figures

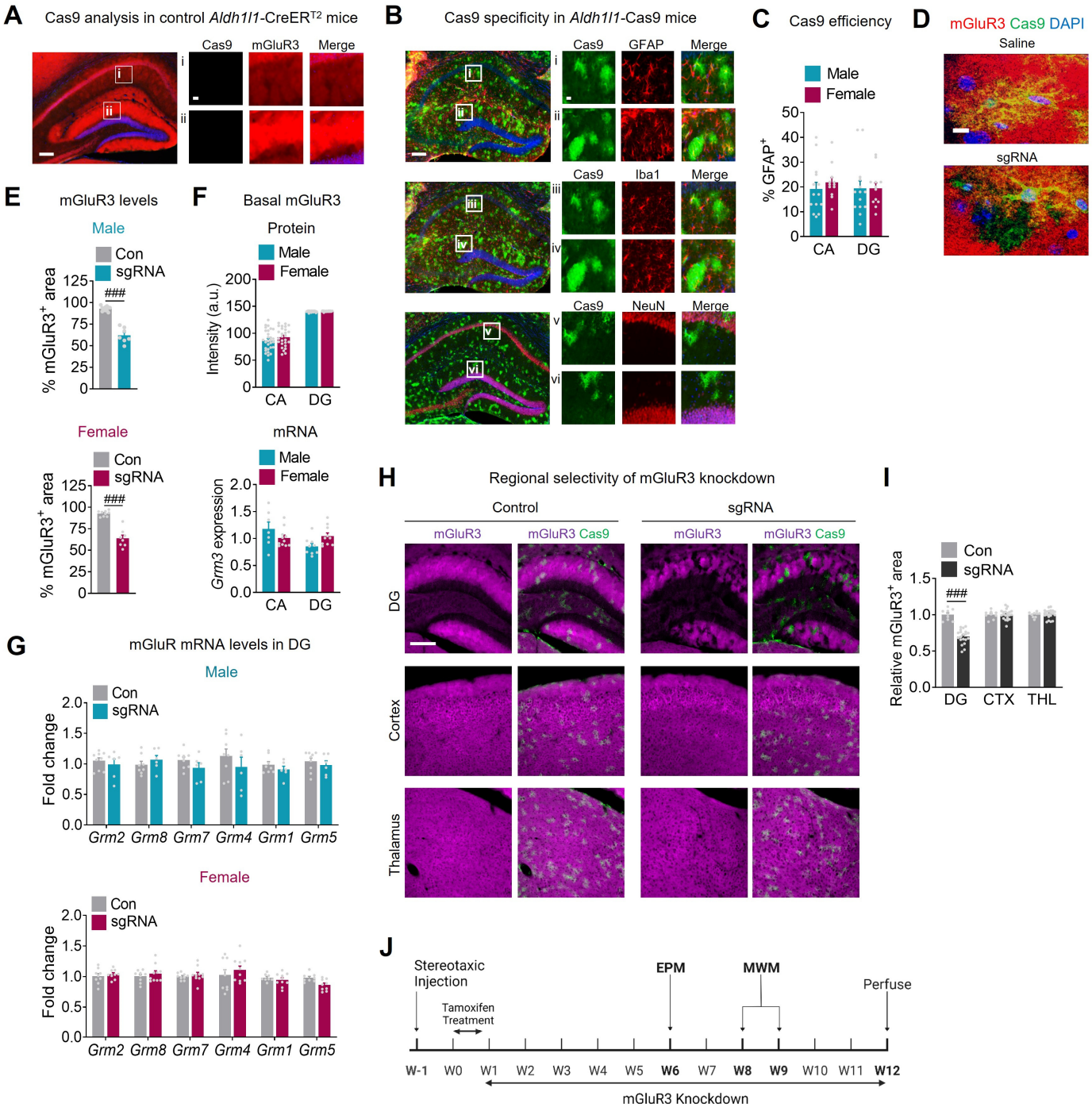

Figure S1. Further characterization of *Aldh1l1*-Cas9 mice and mGluR levels. Related to Figure 1. (**A**) mGluR3 (red) and Cas9-eGFP (green) co-immunolabeling from the CA1 stratum radiatum (CA1sr, i) and DG molecular layer (DGmol) (ii) in sgRNA-injected *Aldh1l1*-CreER^{T2} single transgenic control mice. Scale bars: 400 μm, 40 μm (insets). (**B**) Cas9-eGFP (green) co-immunolabeling with cell type-specific markers (red), including GFAP for astrocytes (i, ii), Iba1 for microglia/macrophages (iii, iv), and NeuN for neurons (v, vi) in *Aldh1l1*-Cas9 double transgenic mice treated with tamoxifen (TAM). DAPI (blue) labeled cell nuclei. Scale bars: 400 μm, 40 μm (insets). (**C**) Immunofluorescence-based quantification of the percentage of GFAP-positive cells that were also Cas9-eGFP-positive in the CA1sr and DGmol regions of the hippocampus

of TAM-injected *Aldh1l1*-Cas9 mice. (**D**) mGluR3 (red) and Cas9-eGFP (green) co-immunolabeling in saline or sgRNA-injected *Aldh1l1*-Cas9 mice. Images highlight astrocytic loss of mGluR3 in Cas9-positive cells in the dentate gyrus (DG). Scale bar: 10 μm (**E**) Immunofluorescence-based quantification of the % DG area that was mGluR3-positive in saline-injected (Con) and sgRNA-injected *Aldh1l1*-Cas9 mice treated with TAM. Two-way ANOVA: $F(1, 31) = 39.40$, $p < 0.001$ for main effect of sgRNA; $F(1, 31) = 0.59$, $p = 0.45$ for interaction effect. (**F**) Immunofluorescence-based (protein) and RT-qPCR-based (mRNA) quantification of mGluR3 levels in the CA and DG regions of saline-treated male and female mice. Two-way ANOVA (Protein): $F(1, 48) = 0.28$, $p = 0.60$ for main effect of sex. Two-way ANOVA (mRNA): $F(1, 33) = 0.03$, $p = 0.86$ for main effect of sex. (**G**) RNA levels of different mGluR subtypes in the DG region of mice with or without mGluR3 knockdown, shown in the order of sequence homology to mGluR3. Three-way ANOVA: $F(5, 173) = 1.01$, $p = 0.41$ for interaction effect. (**H**) mGluR3 (magenta) and Cas9-eGFP (green) co-immunolabeling in saline- or sgRNA-injected *Aldh1l1*-Cas9 mice. Images highlight astrocytic loss of mGluR3 in Cas9-positive cells in the dentate gyrus (DG), but not in the neocortex or thalamus. Scale bar: 200 μm. (**I**) Immunofluorescence-based quantification of mGluR3 expression across brain regions, including the DG, neocortex (CTX), and thalamus (THL) in saline or sgRNA-injected *Aldh1l1*-Cas9 mice. Two-way ANOVA: $F(2, 83) = 37.72$, $p < 0.0001$ for interaction effect. (**J**) Experimental timeline for mice with astrocytic mGluR3 knockdown. Sidak's multiple comparisons post-hoc test (E, F, G, I): $^{###}p < 0.001$. Data are represented as mean ± SEM. See Table S3 for replicate details.

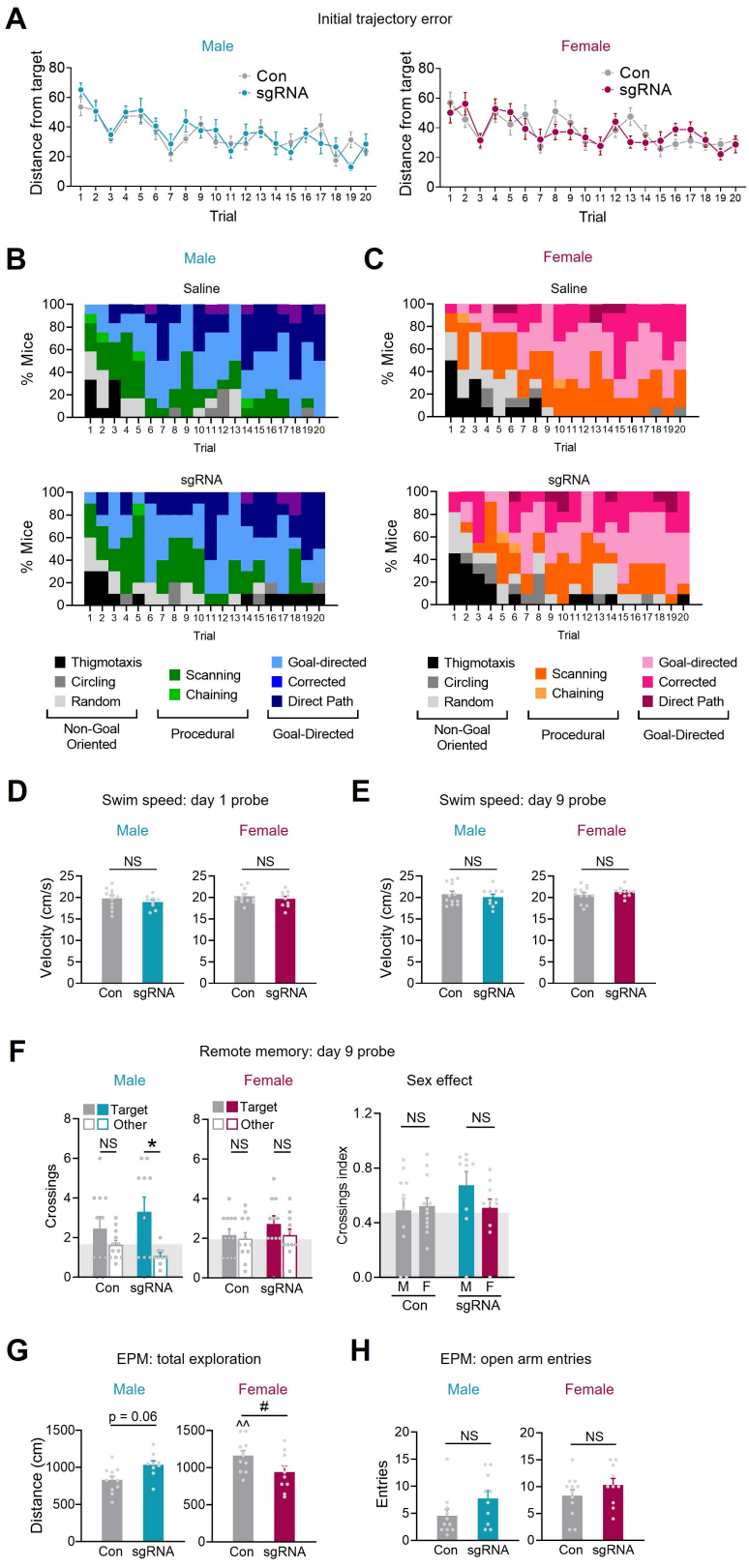

Figure S2. Additional behavioral characterization of *Aldh1l1*-Cas9 mice with or without mGluR3 knockdown in hippocampal astrocytes. Related to Figure 1. (**A**) Initial trajectory errors in male and female mice during training. Three-way ANOVA: $F(19, 820) = 1.07$, $p = 0.38$ for interaction effect. (**B**, **C**) Search strategies in male and female mice during training. (**D**, **E**) Swim speeds in probe trials conducted one (D) and nine (E) days post-training. Two-way ANOVA: $F(1, 38) = 0.03$, $p = 0.85$ for interaction effect (D); $F(1, 40) = 1.17$, $p = 0.29$ for interaction effect (E). (**F**) Target platform crossings as compared to other analogous

locations during a probe trial performed nine days after training. Target preferences were compared using Student's t-tests:*$p < 0.05$. Index values were analyzed using a two-way ANOVA with Sidak's multiple comparisons post-hoc test. Two-way ANOVA (crossings index): $F(1, 39) = 1.59$, $p = 0.215$ for interaction effect. (**G**) Exploration in the elevated plus maze (EPM). Two-way ANOVA: $F(1, 37) = 10.88$, $p = 0.0022$ for treatment/sex interaction effect. (**H**) Open-arm entries in the EPM. Two-way ANOVA: $F(1, 39) = 0.23$, $p = 0.63$ for interaction effect. Three-way (A) or two-way ANOVA with Sidak's multiple comparisons or Tukey's post-hoc tests: $^{\#}p < 0.05$; Sidak's post-hoc test (vs. male/saline group): ^^$p < 0.01$. NS: not significant. Data in panels A and D–H are represented as mean ± SEM. See Table S3 for replicate details.

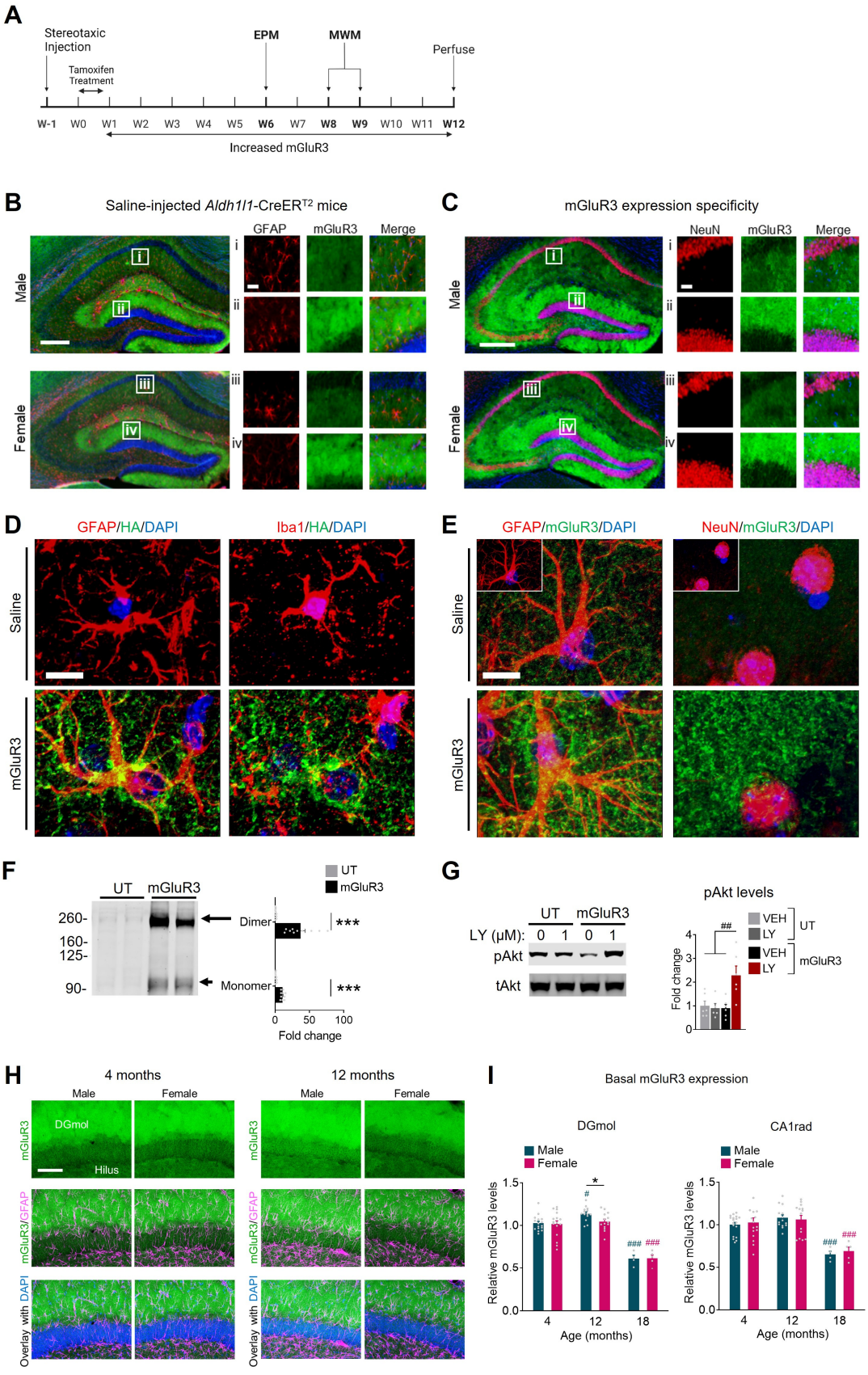

Figure S3. Hippocampal mGluR3 expression levels and validation of AAV vector encoding HA-tagged mGluR3. Related to Figure 2. (**A**) Experimental timeline for mice with increased astrocytic mGluR3 expression. (**B**) mGluR3 (green) and GFAP (red) co-immunolabeling in the hippocampus of saline-injected (control) *Aldh1l1*-CreER^{T2} male and female mice imaged with longer exposure (as shown in insets included in

main Figure 2). DAPI (blue) labeled cell nuclei. Scale bars: 400 µm, 40 µm (insets). (**C**) mGluR3 (green) and NeuN (red) co-immunolabeling in the CA1 and DG of AAV vector-injected *Aldh1l1*-CreER^{T2} male and female mice. Scale bars: 400 µm, 40 µm (insets). (**D**) HA-mGluR3 (green) and GFAP or Iba1 (red) co-immunolabeling in the DG of *Aldh1l1*-CreER^{T2} mice injected with either saline or mGluR3-encoding AAV vector. DAPI (blue) labeled cell nuclei. Scale bar: 10 µm. (**E**) Total mGluR3 expression (green) and GFAP (astrocyte, red) or NeuN (neuron, red) co-immunolabeling in the DG of *Aldh1l1*-CreER^{T2} mice injected with either saline or mGluR3-encoding AAV vector. Inherent differences in mGluR3 intensities required the use of different image acquisition and processing settings. Insets show images of saline-injected mice in which mGluR3 signal was processed similarly to mice with AAV injections. Scale bar: 10 µm. (**F**) Representative Western blot and quantification of mGluR3 dimers and monomers in primary cultured astrocytes untransduced (UT) or transduced with a Cre-dependent AAV vector encoding mGluR3. Experiments were performed in two independent cultures. Student's t-test: ***$p < 0.001$. (**G**) Representative Western blots and quantification of phosphorylated Akt and total Akt levels following mGluR3 stimulation with LY354740 (LY, 1 µM, 10 min) in cultured astrocytes that were untransduced (UT) or transduced with a Cre-dependent AAV vector encoding mGluR3. Experiments were performed in two independent cultures. Two-way ANOVA of pAkt: $F(1, 19) = 8.16$, $p = 0.01$ for interaction effect. Sidak's multiple comparisons post-hoc test (vs Veh): $^{\#\#}p < 0.01$. (**H**) Co-immunolabeling for mGluR3 (green) and astrocyte marker GFAP (magenta) in the hippocampus of nontransgenic male and female mice at 4 and 12 months of age. DAPI (blue) labeled cell nuclei. Scale bar: 100 µm. (**I**) Quantification of mGluR3 immunolabeling in the indicated regions of the hippocampus of nontransgenic males and females at three different ages. Data were normalized to 4-month-old males per brain region. Student's t-test (males vs. females per age group): *$p < 0.05$. Two-way ANOVA (DGmol): $F(2, 63) = 66.88$, $p < 0.0001$ for age effect. Sidak's multiple comparisons post-hoc test: $^{\#}p < 0.05$, $^{\#\#\#}p < 0.0001$ (vs. 4 months of age per sex). Two-way ANOVA (CA1rad): $F(2, 65) = 21.64$, $p < 0.0001$ for age effect. Sidak's multiple comparisons post-hoc test: $^{\#\#\#}p < 0.0001$ (vs. 4 months of age per sex). Data in panels F, G, and I are represented as mean ± SEM. See Table S3 for replicate details.

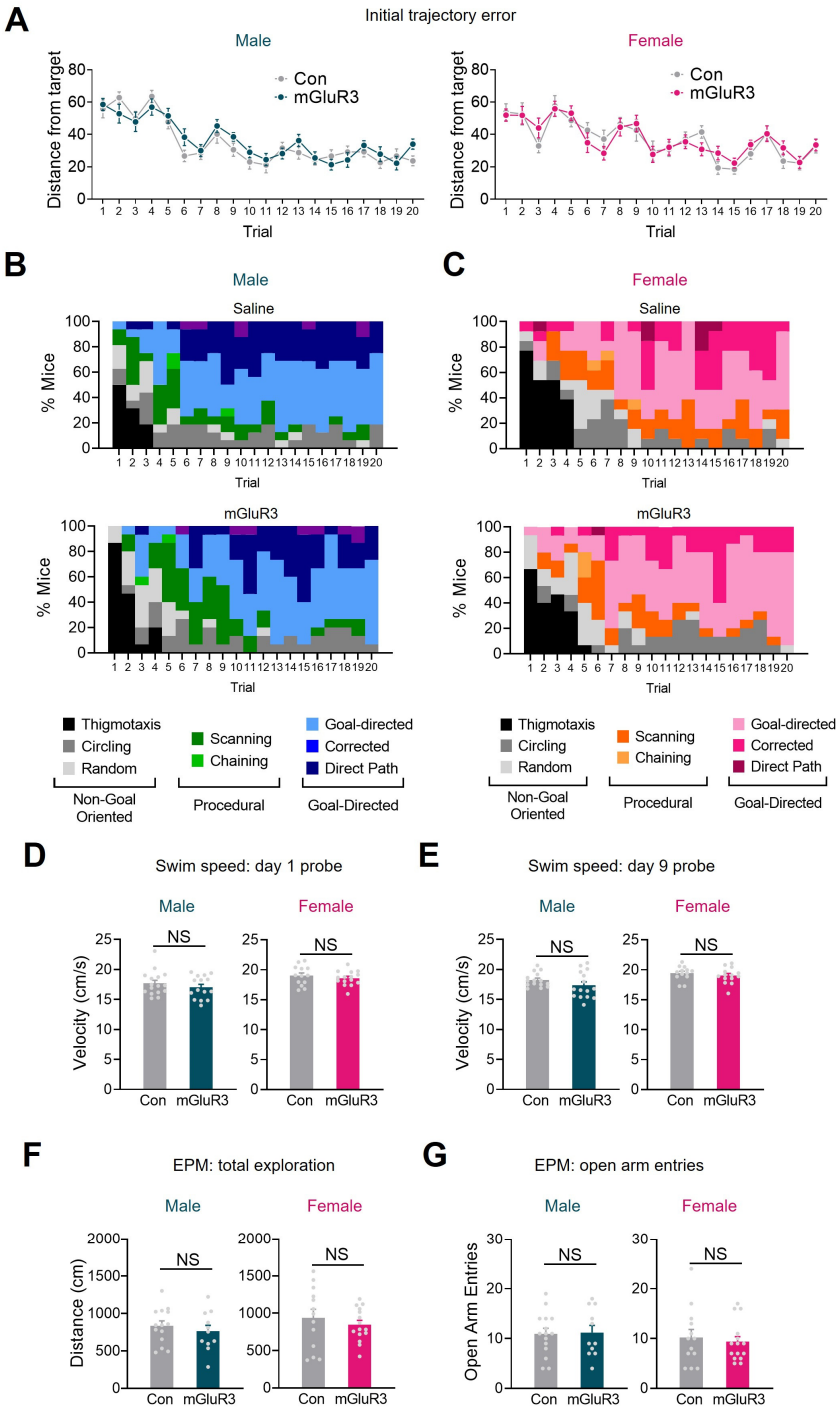

Figure S4. Additional behavioral characterization of *Aldh1l1*-CreER^{T2} mice with or without enhancement in astrocytic mGluR3 expression. Related to Figure 2. (**A**) Initial trajectory errors during training in male and female *Aldh1l1*-CreER^{T2} mice after injection with mGluR3-encoding AAV vector or saline (Con). Three-way ANOVA: $F(19, 1045) = 1.27$, $p = 0.19$ for interaction effect. (**B**, **C**) Search strategies in male and female mice during training. (**D**, **E**) Swim speeds in male and female mice during probe trial at one day (D) and nine days (E) post-training. (**F**) Distance traveled in the elevated plus maze (EPM). Two-way ANOVA: $F(1, 49) = 1.04$, $p = 0.31$ for interaction effect. (**G**) Open-arm entries in the EPM. Two-way ANOVA: $F(1, 50) = 0.19$, $p = 0.66$ for interaction effect. Data in (A) were analyzed with a three-way ANOVA and Tukey's post-hoc test. Data in (D, E, F, G) were analyzed with a two-way ANOVA and Sidak's multiple comparisons post-hoc test. NS: not significant. Data in panels A and D–G are represented as mean ± SEM. See Table S3 for replicate details.

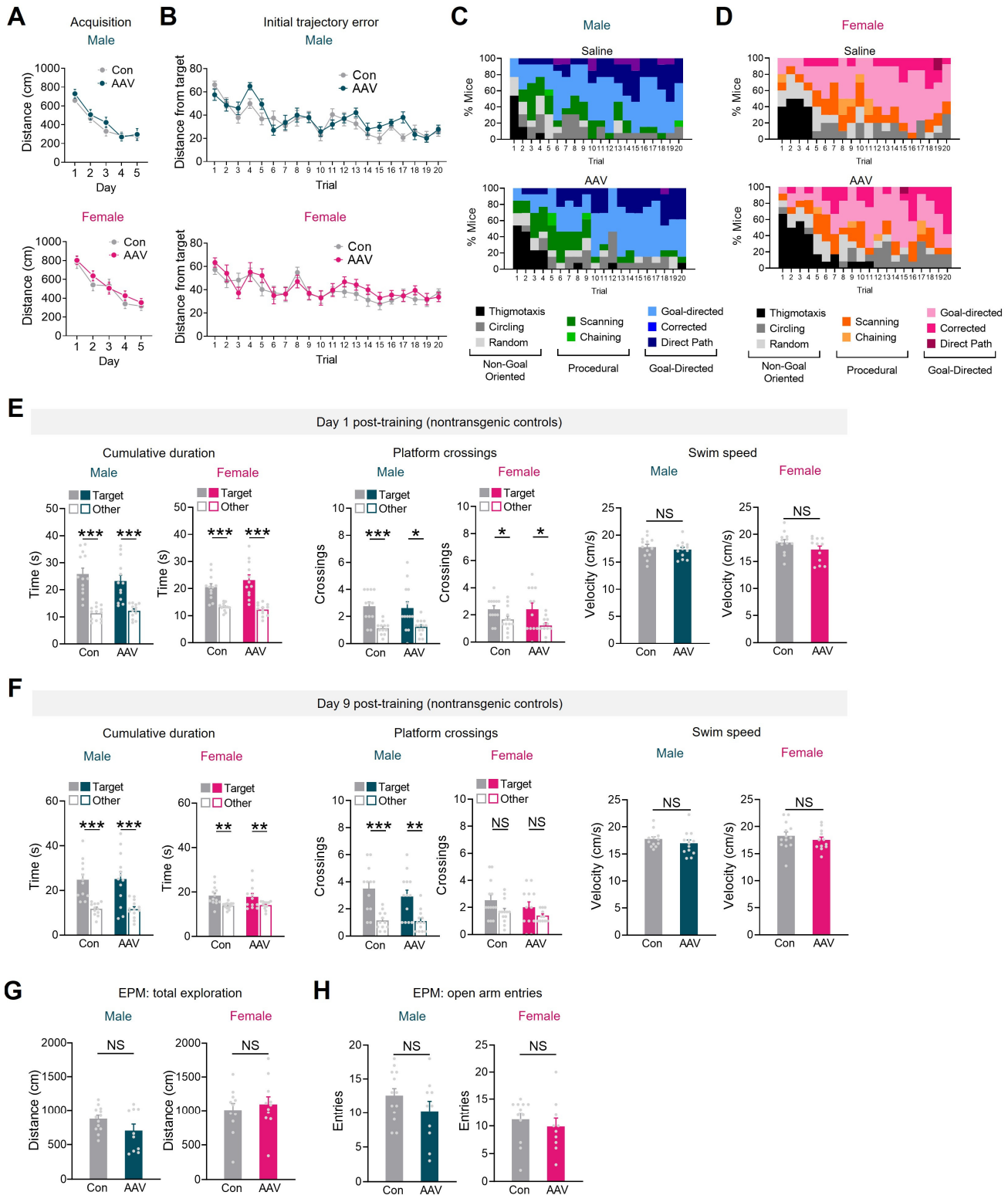

Figure S5. Lack of effects from AAV vector injections on behavioral readouts in nontransgenic control littermates of *Aldh1l1*-CreER^{T2} mice. Related to Figure 2. (**A**) Distance to reach the platform during training in male and female nontransgenic mice injected with saline or Cre-dependent mGluR3-encoding AAV vector. Three-way ANOVA: $F(9, 432) = 0.72$, $p = 0.69$ for interaction effect. (**B**) Initial trajectory errors of male and female mice during training. Three-way ANOVA: $F(19, 896) = 1.008$, $p = 0.45$ for interaction effect. (**C**, **D**) Search strategies of male and female mice during training. (**E**) Quadrant durations in target and non-target quadrants (two-way ANOVA: $F(1, 46) = 1.9$, $p = 0.18$ for interaction effect); number of target and non-target platform crossings (two-way ANOVA: $F(1, 45) = 0.03$, $p = 0.87$ for interaction effect);

swim speeds during probe trial. (**F**) Quadrant durations in target and non-target quadrants (two-way ANOVA: $F(1, 46) = 0.04$, $p = 0.84$ for interaction effect); number of target and non-target platform crossings (two-way ANOVA: $F(1, 46) = 0.002$, $p = 0.97$ for interaction effect); swim speeds during probe trial. (**G**) Distance traveled in the EPM by nontransgenic male and female mice with or without (Con) injection with the mGluR3-encoding AAV vector. Two-way ANOVA: $F(1, 41) = 2.09$, $p = 0.16$ for interaction effect. (**H**) Open-arm entries in the EPM by nontransgenic male and female mice with or without AAV vector injections. Two-way ANOVA: $F(1, 41) = 0.18$, $p = 0.68$ for interaction effect. Data were analyzed with a three-way ANOVA and Tukey's post-hoc test (A, B), two-way ANOVA and Sidak's multiple comparisons post-hoc test (G, H), or a Student's t-test (E, F): *$p < 0.05$, **$p < 0.01$, ***$p < 0.001$, NS: not significant. Data in all panels except C and D are represented as mean ± SEM. See Table S3 for replicate details.

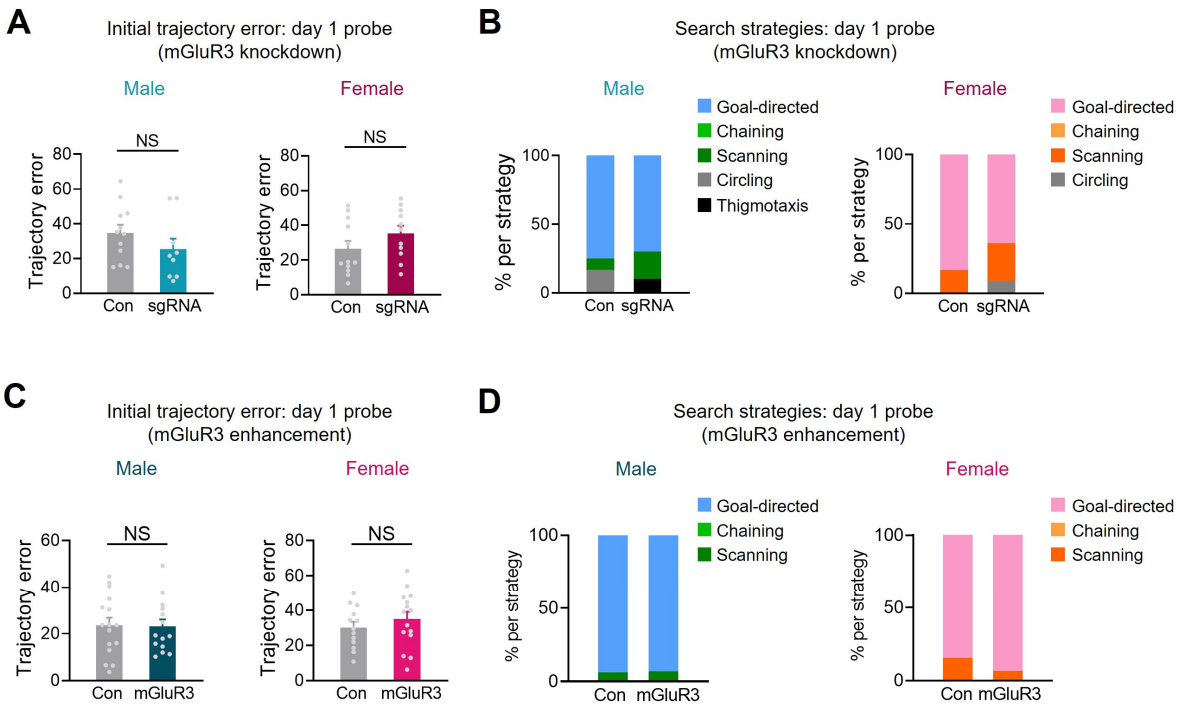

Figure S6. Trajectories and spatial search strategies in early probe trials after knockdown or enhancement of astrocytic mGluR3 levels. Related to Figure 3. Initial trajectory errors (A, C) and search strategies (B, D) in probe trials performed one day after training in male and female mice with either reduced (A, B) or enhanced (C, D) mGluR3 in hippocampal astrocytes. Data in (A, C) were analyzed with two-way ANOVA and Sidak's post-hoc tests. Data in (B, D) were analyzed with Fisher's exact test. NS: not significant. Data in panels A and C are represented as mean ± SEM. See Table S3 for replicate details.

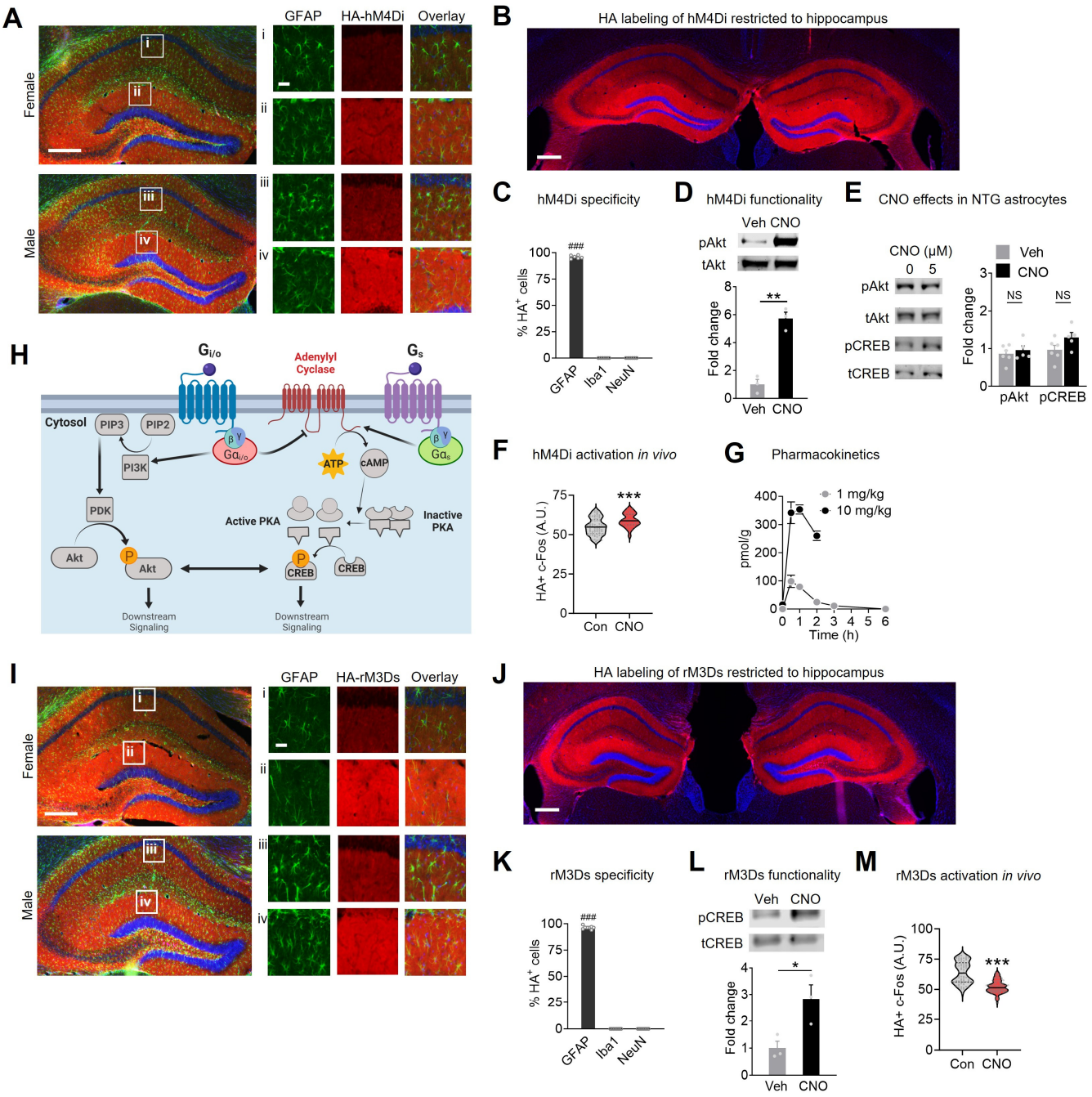

Figure S7. Characterization of astrocyte-targeted hM4Di- and rM3Ds-encoding AAV vectors and CNO pharmacokinetics. Related to Figure 4. (**A**) Astrocyte marker GFAP (green) and HA-hM4Di (red) co-immunolabeling in hippocampal sections from *Aldh1l1*-Cre male and female mice injected with AAV vector encoding HA-tagged hM4Di. DAPI (blue) labeled cell nuclei. Scale bars: 400 μm, 40 μm (insets). (**B**) HA-hM4Di (red) immunolabeling in hippocampal sections from *Aldh1l1*-Cre mice. HA labeling was robust in the hippocampal formation, the region where the AAVs were injected, but minimal in brain regions outside of the hippocampus. Scale bar: 400 μm. (**C**) Immunofluorescence-based quantification of the percentage of GFAP-positive, Iba1-positive, and NeuN-positive cells that were also HA-positive in the hippocampus of *Aldh1l1*-Cre mice injected with AAV vectors encoding HA-hM4Di. One-way ANOVA: $F(2, 15) = 23467$, $p < 0.0001$ for cell marker effect. Dunnett's multiple comparisons test: $^{###}p < 0.0001$, GFAP+ vs. others. (**D**) Phospho-Akt levels following hM4Di stimulation with CNO (5 μM) in primary astrocytes. Data collected from one culture. (**E**) CNO does not cause significant increases in Akt or CREB phosphorylation levels in control astrocytes without AAV transduction. Data collected from two independent cultures. Two-way ANOVA and Sidak's multiple

comparisons post-hoc test. NS: not significant. (**F**) Quantification of c-Fos immunolabeling in HA-positive cells in *Aldh1l1*-Cre mice injected with AAV vectors encoding HA-hM4Di and then injected i.p. with CNO (1 h; 5 mg/kg) or saline (Con). (**G**) Pharmacokinetic analyses of clozapine and CNO in the hippocampal formation following peripheral CNO injection (i.p.) in adult mice at indicated doses. In concurrence with previous findings, CNO was not detectable in the brain, likely due to rapid conversion to clozapine [S1, S2]. (**H**) Simplified diagram of several previously characterized signaling cascades engaged by $G_{i/o}$-coupled and G_s-coupled GPCRs and their mutual regulation. (**I**) Co-immunolabeling for GFAP (green) and HA-rM3Ds (red) in mouse hippocampal sections from *Aldh1l1*-Cre female and male mice injected with AAV vector encoding HA-tagged rM3Ds. Scale bar: 400 μm, 40 μm (insets). (**J**) HA-rM3Ds (red) immunolabeling in hippocampal sections from *Aldh1l1*-Cre mice. HA labeling was robust in the hippocampal formation, the region where the AAVs were injected, but minimal in brain regions outside of the hippocampus. Scale bar: 400 μm. (**K**) Immunofluorescence-based quantification of the percentage of GFAP-positive, Iba1-positive, and NeuN-positive cells that were also HA-positive in the hippocampus of *Aldh1l1*-Cre mice injected with AAV vectors encoding HA-rM3Ds. One-way ANOVA: $F(2, 21) = 32370$, $p < 0.0001$ for cell marker effect. Dunnett's multiple comparisons test: $^{###}p < 0.0001$, GFAP+ vs. others. (**L**) Levels of phosphorylated CREB following rM3Ds stimulation with CNO (5 μM) in cultured astrocytes. Data collected from one culture. Student's t-tests: $^{***}p< 0.001$, $^{**}p < 0.01$, $^{*}p < 0.05$. (**M**) Quantification of c-Fos immunolabeling in HA-positive cells in *Aldh1l1*-Cre mice injected with AAV vectors encoding HA-rM3Ds and then injected i.p. with CNO (1 h; 5 mg/kg) or saline (Con). Data are represented as mean ± SEM, except violin plots in F and M show medians. See Table S3 for replicate details.

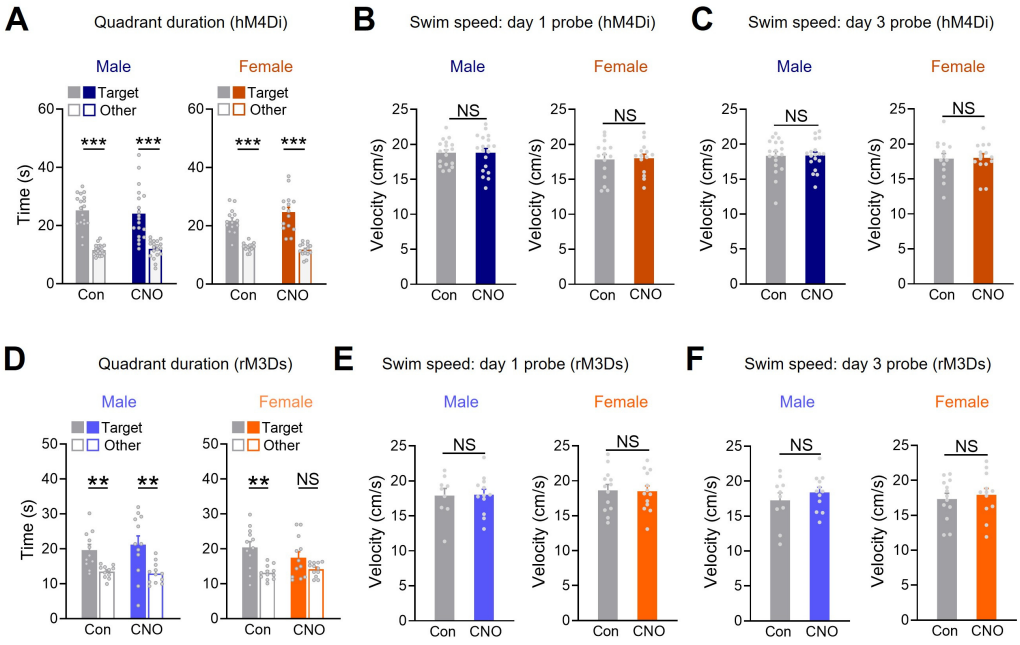

Figure S8. Further behavioral characterization of DREADD-expressing mice. Related to Figure 4. (**A**) Probe trials performed one day after training of hM4Di-expressing mice. Target quadrant durations compared to other analogous locations. Target preferences were compared using Student's t-tests. Student's t-test: ***p < 0.001. (**B**, **C**) Swim speeds in mice expressing hM4Di in hippocampal astrocytes during day one (B) and day three (C) probe trials. Two-way ANOVA: $F(1, 62) = 0.01$, $p = 0.91$ for interaction effect (B), $F(1, 61) = 0.007$, $p = 0.93$ for interaction effect (C). (**D**) Probe trials performed one day after training of rM3Ds-expressing mice. Target quadrant durations compared to other analogous locations. Target preferences were compared using Student's t-tests. Student's t-test: **p < 0.01. NS: no significant preference for target. (**E, F**) Swim speeds in mice expressing rM3Ds in hippocampal astrocytes during day one (E) and day three (F) probe trials. Two-way ANOVA and Sidak's post-hoc test: $F(1, 43) = 0.03$, $p = 0.87$ for interaction effect (E), $F(1, 43) = 0.095$, $p = 0.76$ for interaction effect (F). NS: not significant. Data are represented as mean ± SEM. See Table S3 for replicate details.

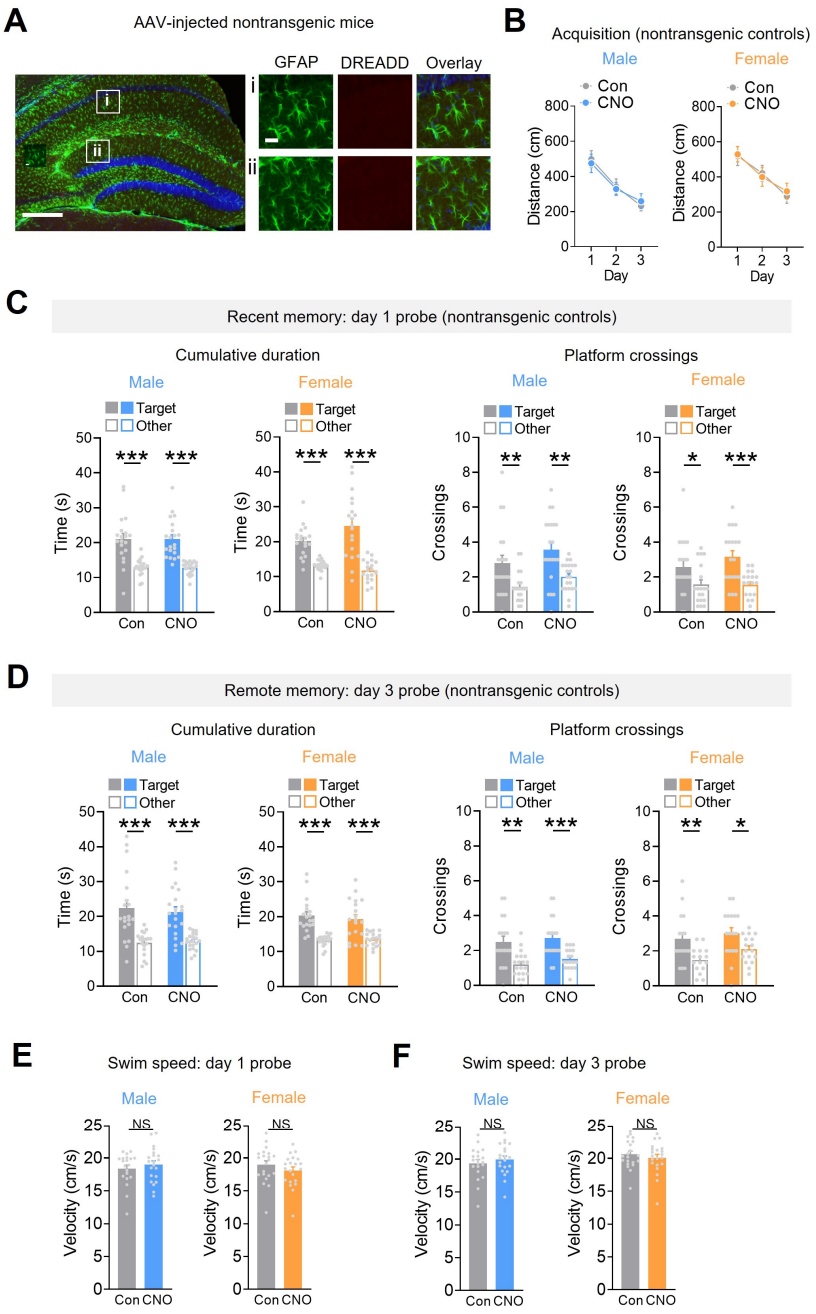

Figure S9. Lack of CNO effects in nontransgenic control mice. Related to Figure 4. (**A**) GFAP (green) and DREADD (red) co-immunolabeling in AAV vector-injected nontransgenic mice used for testing off-target effects of CNO. DREADD labeling was absent in nontransgenic mice. DAPI (blue) labeled cell nuclei. Scale bars: 400 µm, 40 µm (insets). (**B**) Distance to reach the platform during training by vehicle (Con)- or CNO-injected non-transgenic mice. Three-way ANOVA: $F(2, 150) = 0.09$, $p = 0.92$ for interaction effect (time, sex, CNO). (**C**) Target quadrant durations and platform crossings compared to other analogous locations during a probe trial one day after training. Mice were injected with vehicle (Con) or CNO 1 h prior to the training trials and tested off-treatment during probe trials. (**D**) Target quadrant durations and platform crossings compared to other analogous locations during a probe trial three days after training. Data in (C, D) were analyzed with a two-way ANOVA and Student's t-tests to determine target preferences. *$p < 0.05$, **$p < 0.01$, ***$p < 0.001$. (**E**, **F**) Swim speeds during indicated probe trials in nontransgenic mice injected with vehicle or CNO during training. Two-way ANOVA and Sidak's post-hoc test: $F(1, 75) = 1.67$, $p = 0.20$ for interaction effect (E), $F(1, 75) = 0.73$, $p = 0.40$ for interaction effect (F). NS: not significant. Data are represented as mean ± SEM. See Table S3 for replicate details.

Supplemental Tables

Study	Receptor(s)	Sex	Sex effects reported?
G_s			
Orr et al., 2015	Rs1	Males and Females	No assessment of sex differences
Oe et al., 2020	rM3Ds	Males and Females	No assessment of sex differences
$G_{i/o}$			
Jones et al., 2018	hM4Di	Males	N/A
Nagai et al., 2019	hM4Di	Only males in behavior	No assessment of sex differences
Nam et al., 2019	hM4Di	Males	N/A
Kol et al., 2020	hM4Di	Males	N/A
Yu et al., 2020	hM4Di	Only males in behavior	No assessment of sex differences
Akter et al., 2023	hM4Di	Males	N/A
Reitman et al., 2023	hM4Di	Males and Females	No assessment of sex differences
$G_{i/o}$ and G_q			
Yang et al., 2015	hM4Di, hM3Dq	Males	N/A
Kim et al., 2021	hM4Di, hM3Dq	Males	N/A
Vaidyanathan et al., 2021	hM4Di, hM3Dq	Males and Females	No assessment of sex differences
Van Den Herrewegen et al., 2021	hM4Di, hM3Dq	Males	N/A
Refaeli et al., 2024	hM4Di, hM3Dq	Males	N/A
G_q			
Adamsky et al., 2018	hM3Dq	Males	N/A
Nagai et al., 2021	hM3Dq	Males and Females	No assessment of sex differences
Delepine et al., 2023	hM3Dq	Males and Females	No assessment of sex differences

N/A: Sex differences could not be assessed, only one sex included.

Table S1. Summary of males and females assessed in previous *in vivo* studies using chemogenetic manipulations and behavioral measurements. Related to Figures 1–4. Citations in the table are specified in the Supplemental reference list [S3–S19].

Fig #	Panel	Condition	Sex	
			Male	*Female*
1	C (CA1, DG)	GFAP	15	12
		Iba1	17	15
		NeuN	6	6
	D (CA, DG)	Con	6	6
		sgRNA	5	5
	E (CA)	Con	7	11
		sgRNA	8	7
	E (DG)	Con	8	9
		sgRNA	5	10
	G-J	Con	12	12
		sgRNA	10	11
2	C	GFAP, NeuN	9	9
	D (CA, DG)	Con	12	11
		mGluR3	13	15
	E	Con	12	10
		mGluR3	13	14
	F-I	Con	16	12
		mGluR3	15	15
3	A, C, E	Con	12	12
		mGluR3	10	11
	B, D, F	Con	16	12
		mGluR3	15	14
4	C	NA	10	17
	D-F	Con	19	15
		CNO	19	15
	I	NA	8	8
	J-L	Con	12	13
		CNO	12	13

Table S2. Numbers of mice used in each experiment shown in the main figures. Related to Figures 1–4.

Supplemental Fig #	Panel	Condition	Sex	
			Male	*Female*
S1	C	NA	14	12
	E	Con	11	9
		sgRNA	7	8
	F	Protein	6	6
		mRNA	9	11
	G	Con	9	9
		sgRNA	6	10
	I	Con	1	1
		sgRNA	1	3
S2	A-E	Con	12	12
		sgRNA	10	11
	F	Con	12	12
		sgRNA	10	11
	G	Con	11	11
		sgRNA	9	10
	H	Con	12	12
		sgRNA	10	10
S3	I	4 mos-DGmol	16	16
		12 mos-DGmol	14	14
		18 mos-DGmol	4	5
		4 mos-CA1rad	18	16
		12 mos-CA1rad	14	14
		18 mos-CA1rad	4	5
S4	A-E	Con	16	12
		mGluR3	15	14
	F-G	Con	15	13
		mGluR3	11	15
S5	A-F	Con	13	13
		mGluR3	14	12
	G-H	Con	13	11
		mGluR3	10	11
S6	A-B	Con	12	12
		sgRNA	11	9
	C-D	Con	16	13
		mGluR3	14	15
S7	C	NA	0	3
	F	Con	3	3
		CNO	2	2
	G	1 mg/kg	3-4/timepoint	
		10 mg/kg	3-4/timepoint	
	K	NA	3	1
	M	Con	3	3
		CNO	3	4
S8	A-C	Con	19	15
		CNO	19	15
	D-F	Con	9	13
		CNO	12	13
S9	B-F	Con	21	19
		CNO	21	19

Table S3. Numbers of mice used in each experiment shown in the supplemental figures. Related to Figures S1–S9.

Gene	Forward primer	Reverse primer
Grm1	GCAGCGAGCCTTGCTTAAA	AGATCCAGCAGCAGCTCAC
Grm2	GGACTTCGTGCTCAATGTCA	CCATCTCCAAAGCGGTCAAA
Grm3	ACCTCAACAGGTTCAGTGTCA	TTGCACACTGTCGGGACATA
Grm4	TCAAGAAGGGAAGCCACATCAA	ACCTTCCCCTCCTGTTCGTA
Grm5	TGCAGTGAACCGTGTGAGAA	AAGGTGTGCAGGTCCAACAA
Grm7	AAGGAGCCATCACCATCCAA	TCAAGTGTCCGGGATGTGAA
Grm8	CCACTGGACCAATCAACTTCAC	GGGTGCGTGTGCTCTCTATTA
Actb	CCCTAAGGCCAACCGTGAAA	AGCCTGGATGGCTACGTACA
Gapdh	CAAGGTCATCCCAGAGCTGAA	CAGATCCACGACGGACACA
Gusb	AGTATGGAGCAGACGCAATCC	ACAGCCTTCTGGTACTCCTCA
Tbp	CCTTGTACCCTTCACCAATGAC	ACAGCCAAGATTCACGGTAGA

Table S4. Primer sequences used for RT-qPCR. Related to STAR Methods.

Supplemental References

[S1] Gomez, J.L., Bonaventura, J., Lesniak, W., Mathews, W.B., Sysa-Shah, P., Rodriguez, L.A., Ellis, R.J., Richie, C.T., Harvey, B.K., Dannals, R.F., et al. (2017). Chemogenetics revealed: DREADD occupancy and activation via converted clozapine. Science *357*, 503-507. 10.1126/science.aan2475.

[S2] Raper, J., Morrison, R.D., Daniels, J.S., Howell, L., Bachevalier, J., Wichmann, T., and Galvan, A. (2017). Metabolism and Distribution of Clozapine-N-oxide: Implications for Nonhuman Primate Chemogenetics. ACS Chem Neurosci *8*, 1570-1576. 10.1021/acschemneuro.7b00079.

[S3] Orr, A.G., Hsiao, E.C., Wang, M.M., Ho, K., Kim, D.H., Wang, X., Guo, W., Kang, J., Yu, G.Q., Adame, A., et al. (2015). Astrocytic adenosine receptor A2A and Gs-coupled signaling regulate memory. Nat Neurosci *18*, 423-434. 10.1038/nn.3930.

[S4] Yang, L., Qi, Y., and Yang, Y. (2015). Astrocytes control food intake by inhibiting AGRP neuron activity via adenosine A1 receptors. Cell Rep *11*, 798-807. 10.1016/j.celrep.2015.04.002.

[S5] Adamsky, A., Kol, A., Kreisel, T., Doron, A., Ozeri-Engelhard, N., Melcer, T., Refaeli, R., Horn, H., Regev, L., Groysman, M., et al. (2018). Astrocytic Activation Generates De Novo Neuronal Potentiation and Memory Enhancement. Cell *174*, 59-71 e14. 10.1016/j.cell.2018.05.002.

[S6] Jones, M.E., Paniccia, J.E., Lebonville, C.L., Reissner, K.J., and Lysle, D.T. (2018). Chemogenetic Manipulation of Dorsal Hippocampal Astrocytes Protects Against the Development of Stress-enhanced Fear Learning. Neuroscience *388*, 45-56. 10.1016/j.neuroscience.2018.07.015.

[S7] Nagai, J., Rajbhandari, A.K., Gangwani, M.R., Hachisuka, A., Coppola, G., Masmanidis, S.C., Fanselow, M.S., and Khakh, B.S. (2019). Hyperactivity with Disrupted Attention by Activation of an Astrocyte Synaptogenic Cue. Cell *177*, 1280-1292 e1220. 10.1016/j.cell.2019.03.019.

[S8] Nam, M.H., Han, K.S., Lee, J., Won, W., Koh, W., Bae, J.Y., Woo, J., Kim, J., Kwong, E., Choi, T.Y., et al. (2019). Activation of Astrocytic mu-Opioid Receptor Causes Conditioned Place Preference. Cell Rep *28*, 1154-1166 e1155. 10.1016/j.celrep.2019.06.071.

[S9] Kol, A., Adamsky, A., Groysman, M., Kreisel, T., London, M., and Goshen, I. (2020). Astrocytes contribute to remote memory formation by modulating hippocampal-cortical communication during learning. Nat Neurosci *23*, 1229-1239. 10.1038/s41593-020-0679-6.

[S10] Oe, Y., Wang, X., Patriarchi, T., Konno, A., Ozawa, K., Yahagi, K., Hirai, H., Tsuboi, T., Kitaguchi, T., Tian, L., et al. (2020). Distinct temporal integration of noradrenaline signaling by astrocytic second messengers during vigilance. Nat Commun *11*, 471. 10.1038/s41467-020-14378-x.

[S11] Yu, X., Nagai, J., Marti-Solano, M., Soto, J.S., Coppola, G., Babu, M.M., and Khakh, B.S. (2020). Context-Specific Striatal Astrocyte Molecular Responses Are Phenotypically Exploitable. Neuron *108*, 1146-1162 e1110. 10.1016/j.neuron.2020.09.021.

[S12] Kim, J.H., Rahman, M.H., Lee, W.H., and Suk, K. (2021). Chemogenetic stimulation of the G(i) pathway in astrocytes suppresses neuroinflammation. Pharmacol Res Perspect *9*, e00822. 10.1002/prp2.822.

[S13] Nagai, J., Bellafard, A., Qu, Z., Yu, X., Ollivier, M., Gangwani, M.R., Diaz-Castro, B., Coppola, G., Schumacher, S.M., Golshani, P., et al. (2021). Specific and behaviorally consequential astrocyte G(q) GPCR signaling attenuation in vivo with ibetaARK. Neuron *109*, 2256-2274 e2259. 10.1016/j.neuron.2021.05.023.

[S14] Vaidyanathan, T.V., Collard, M., Yokoyama, S., Reitman, M.E., and Poskanzer, K.E. (2021). Cortical astrocytes independently regulate sleep depth and duration via separate GPCR pathways. Elife *10*. 10.7554/eLife.63329.

[S15] Van Den Herrewegen, Y., Sanderson, T.M., Sahu, S., De Bundel, D., Bortolotto, Z.A., and Smolders, I. (2021). Side-by-side comparison of the effects of Gq- and Gi-DREADD-mediated astrocyte modulation on intracellular calcium dynamics and synaptic plasticity in the hippocampal CA1. Mol Brain *14*, 144. 10.1186/s13041-021-00856-w.

[S16] Akter, M., Hasan, M., Ramkrishnan, A.S., Iqbal, Z., Zheng, X., Fu, Z., Lei, Z., Karim, A., and Li, Y. (2023). Astrocyte and L-lactate in the anterior cingulate cortex modulate schema memory and neuronal mitochondrial biogenesis. Elife *12*. 10.7554/eLife.85751.

[S17] Reitman, M.E., Tse, V., Mi, X., Willoughby, D.D., Peinado, A., Aivazidis, A., Myagmar, B.E., Simpson, P.C., Bayraktar, O.A., Yu, G., and Poskanzer, K.E. (2023). Norepinephrine links astrocytic activity to regulation of cortical state. Nat Neurosci *26*, 579-593. 10.1038/s41593-023-01284-w.

[S18] Delepine, C., Shih, J., Li, K., Gaudeaux, P., and Sur, M. (2023). Differential Effects of Astrocyte Manipulations on Learned Motor Behavior and Neuronal Ensembles in the Motor Cortex. J Neurosci *43*, 2696-2713. 10.1523/JNEUROSCI.1982-22.2023.

[S19] Refaeli, R., Kreisel, T., Yaish, T.R., Groysman, M., and Goshen, I. (2024). Astrocytes control recent and remote memory strength by affecting the recruitment of the CA1-->ACC projection to engrams. Cell Rep *43*, 113943. 10.1016/j.celrep.2024.113943.